

*Title : will be set by the publisher*

*Editors : will be set by the publisher*

*EAS Publications Series, Vol. ?, 2009*

## EVOLUTION OF IR DETECTION AND POSSIBLE OUTCOMES FOR ASTROPHYSICS

G. Finger<sup>1</sup>, R. Dorn, L. Mehrgan, M. Meyer and J. Stegmeier

**Abstract.** Infrared focal plane technology has evolved rapidly in the past two decades. The detector format has grown from single pixel detectors to 4Kx4K pixel arrays, and a mosaic of 4x4 2Kx2K pixel arrays and six mosaics of 2x2 2Kx2K pixel arrays are already in operation at ground based telescopes. The quantum efficiency of these arrays is close to 100%, the readout noise a few electrons rms and the dark current a few electrons per hour. However, the latent image problem has not been solved yet. A persistence model and a mitigation strategy will be discussed briefly. Specialized ASIC readout chips which digitize the multichannel video signals of large arrays directly on the focal plane are becoming available for large format arrays and they will eventually replace conventional controllers. In the mid infrared a high flux version of the MIRI detector is being developed for ground based applications. Fast low noise infrared sensors are needed for wavefront sensors of adaptive optics (AO) systems. To meet both the speed and the noise requirements two different technical approaches are being followed. One solution is the use of high gain CTIA amplifiers in the detector unit cell, the other solution is to exploit the noiseless gain mechanism of HgCdTe electron avalanche photodiode (eAPD) arrays.

### 1 Introduction

Large format arrays have undergone a rapid development both in format and in pixel performance. Today 2Kx2K arrays are in routine operation at 8 meter telescopes and the maturity of these devices has reached a level such that photon shot noise limited operation is achieved in most observing modes. Mosaics of 4x4 2Kx2K arrays (VIRGO arrays produced by Raytheon) are in operation at the VISTA telescope (Love *et al.* 2006). Presently the format of HgCdTe arrays grown by molecular beam epitaxy (MBE) on a CdZnTe substrate is limited by the

---

<sup>1</sup> European Southern Observatory, Karl-Schwarzschildstrasse 2, D-85748-Garching, phone: +49-89-32006256, email: gfinger@eso.org

maximum available size of substrates. The largest format possible with a pixel size of  $15\ \mu\text{m}$  is 4Kx4K. Arrays of this format are presently being developed at Teledyne.

## 2 Performance of large format near infrared arrays

In the near infrared spectral region between  $\lambda = 1$  and  $2.5\ \mu\text{m}$  large format HgCdTe arrays have become excellent devices. Some performance characteristics and special readout modes will be discussed below.

### 2.1 Quantum efficiency

The quantum efficiency is well above 80% over the whole spectral range (Finger *et al.* 2008). The arrays are grown with molecular beam epitaxy (MBE) on a CdZnTe substrate. The substrate can be removed by a chemical etch. This extends the sensitivity down to the visible and X-ray spectral range. Therefore, the conversion gain of substrate removed HgCdTe arrays can be calibrated with the  $K_\alpha$  line of  $\text{Fe}^{55}$  at  $hc/\lambda = 5.9\text{KeV}$  (Finger *et al.* 2008). However, the number of electrons generated per absorbed photon may depend on the bandgap of HgCdTe at the location of the X-ray absorption for graded bandgap structures. Substrate removed detectors have the big advantage that they do not suffer from fringing, which is a serious problem in high resolution spectrographs. It is caused by interference of multiple reflections at the parallel surfaces of the detector substrate.

### 2.2 Readout noise

The readout noise of the latest Hawaii-2RG arrays is as low as 6.9 erms for single double correlated sampling as shown in the noise histogram on the left side of Figure 1. The improvement of the readout noise from 25.3 erms measured with device #119 to 6.9 erms measured with device #184 was accomplished by improving the contact resistance of the bond pads. For low noise devices the readout noise measured on infrared active pixels is comparable to the noise of the reference pixels at the edge of the array, whereas it was twice as high on early higher noise devices. Applying multiple nondestructive sampling the readout noise can be reduced shown in the right plot of Figure 1. By increasing the number of non-destructive readouts the noise decreases and is as low as 2.4 erms for 64 readouts (32 Fowler pairs).

### 2.3 Dark current

At temperatures below 80 K most  $\lambda_c=2.5\ \mu\text{m}$  HgCdTe Hawaii-2RG detectors have dark currents below  $10^{-2}$  e/s/pixel. The dark current of a substrate removed HgCdTe array was measured to be as low as  $4.2 \cdot 10^{-4}$  e/s/pixel at a detector operating temperature of 81 K and a bias voltage of 1 V. The dark current of  $\lambda_c$

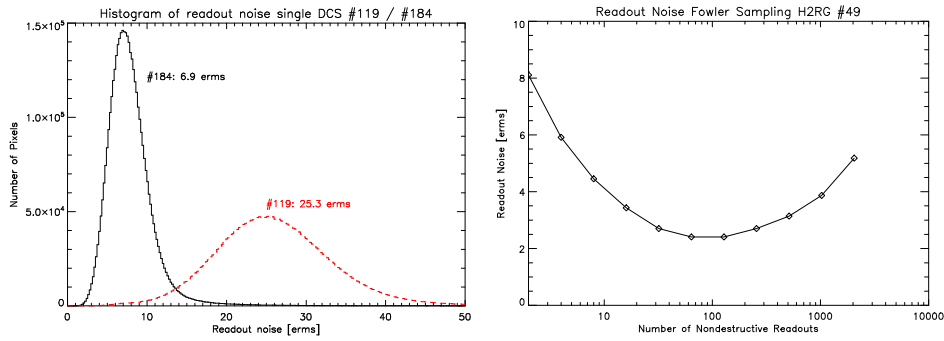


**Fig. 1.** Readout noise of Hawaii-2RG arrays. Left: Noise with single double correlated sampling: array #184: 6.9 erms, array #119: 25.3 erms. Right: Noise with Fowler sampling versus number of nondestructive samples for array #49: 2.4 erms with 32 Fowler pairs.

2.5  $\mu\text{m}$  arrays is dominated by surface generation-recombination Shockley-Hall-Read processes. In this case the dark current is proportional to  $\exp(-E_{gap}/nKT)$  with  $n$  being 2. The parameter  $n$  was determined by measuring the temperature dependence of the dark current. Depending on the specific device it ranges between 1.63 to 1.73 (Finger *et al.* 2008). For diffusion limited dark currents  $n$  is equal to 1. With arrays produced for JWST it has been demonstrated that the dark current of MBE devices having a cut-off wavelength of  $\lambda_c=5\mu\text{m}$  is dominated by a diffusion limited processes down to operating temperatures of 40 K, which clearly is not the case for  $\lambda_c=2.5\mu\text{m}$  Hawaii-2RG arrays (Garnett J. *et al.* 2004).

#### 2.4 Special readout modes

The Hawaii-2RG multiplexer is versatile device. It has a built-in guide window mode. A small guide window can be read at high speed in an interleaved way with the full science frame to correct for atmospheric tip tilt of the wavefront. It has reference pixels for eliminating low frequency noise pickup and thermal drifts.

The sample-up-the-ramp or nondestructive readout mode offers a simple way to expand the dynamic range of the detector for long integration times, which we call TLI (Threshold Limited Integration). The method only requires the definition of a threshold level in ADU units which is below the detector saturation. All pixel values below this threshold are processed normally (pixel with blue integration ramp in the left plot of Figure 2). Pixels values above (e.g. those illuminated by a bright sources) are no longer taken into account for calculating the slope of the integration ramp (pixel with red integration ramp in Figure 2). For those pixels only nondestructive readouts having values below the threshold are taken into account. The stored pixel value is the value extrapolated to the total integration time. It is calculated from the slope using only non-saturated nondestructive readouts as illustrated in the left plot of Figure 2. The right plot in Figure 2

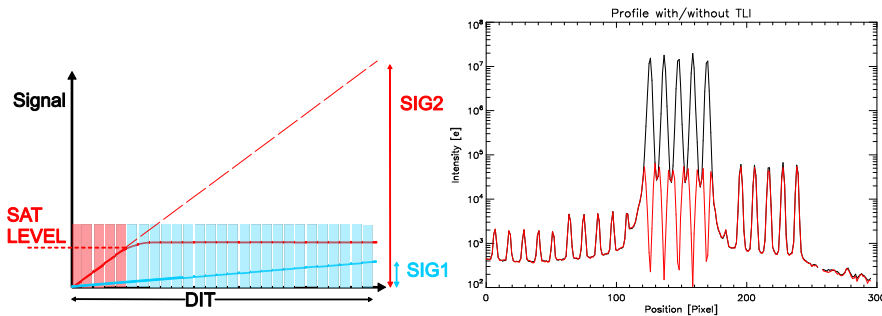


**Fig. 2.** Threshold limited integration (TLI). Left: Saturation threshold for nondestructive sampling and extrapolation of detector signal for high flux levels. For pixels with high flux (red) only pixel values below SATLEVEL are taken into account to calculate the slope. For low flux pixels (blue) all nondestructive readouts indicated by rectangles are used. (for colors see: [www.eso.org/gfinger](http://www.eso.org/gfinger)). Right: Intensity profile of spectral lines with (black) and without (red) TLI. Without TLI lines are saturated. Gain of dynamic range  $> 10^2$ .

shows an intensity profile through bright spectral lines imaged onto the detector and measured with (black curve) and without (red curve) TLI. Without TLI the line centers are saturated. Threshold limited integration is particularly useful for long integration times and can increase the dynamic range of the detector by more than 2 orders of magnitude.

### 3 Persistence of MBE grown HgCdTe DLPH arrays

Both in imaging and especially in spectroscopy with bright atmospheric emission lines and weak spectral lines of distant objects the dynamic range of the detector signal may cover a span of several orders of magnitude. Image persistence, an elevated detector signal at low flux caused by prior exposure to the high flux of bright spectral lines, has been a long standing problem for astronomical observations. The persistent image decays with large time constants, and for low flux applications the persistent image can still be seen hours after the bright illumination has been switched off. There was some hope that changing the growth process of near infrared HgCdTe arrays from liquid phase epitaxy (LPE) to molecular beam epitaxy (MBE) would reduce or even solve the latent image problem. For double layer planar heterostructures (DLPH) of MBE diodes the depletion region of the pn-junction is no longer at the surface of the HgCdTe material as it was in LPE diodes. The diode junction for MBE DLPH diodes is embedded in the bulk of the HgCdTe material with no surface traps and less crystal defects. However, MBE did not eliminate the persistence effect.

The latent charge, or "persistence," is measured as the remaining signal apparent in a series of dark exposures which is produced by a bright source in previous

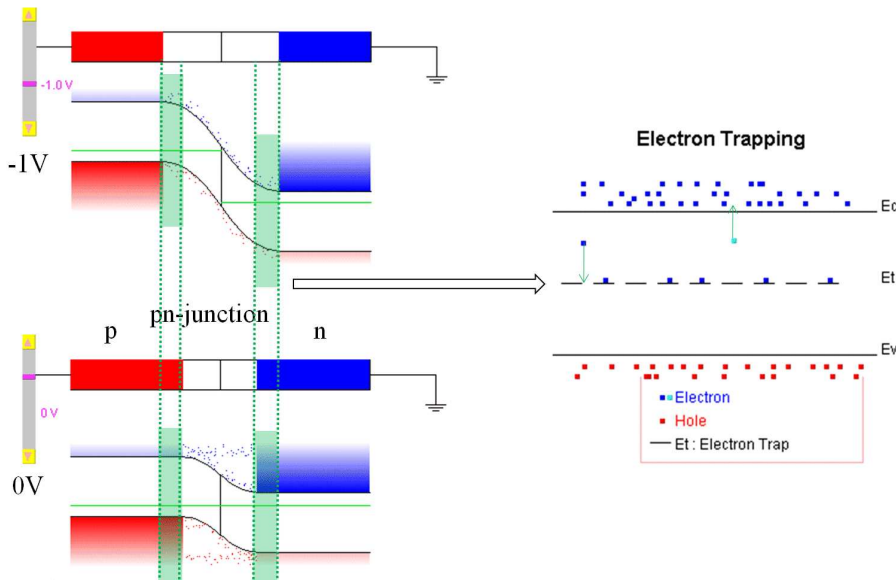


**Fig. 3.** Model of detector persistence. Left side top half: Band diagram for detector bias of  $-1V$  at beginning of integration. Depletion width large. Left side bottom: Band diagram for detector bias of  $0V$  when detector is saturated. Depletion width is narrow. Interband states in green shaded area are exposed to mobile carriers, which may get trapped. Right side: When bias voltage is reset to  $-1V$  during subsequent dark exposures trapped charges are released and seen as persistent image.

images where the detector was exposed to high photon flux levels. Any process which, after some delay, releases charge into the conduction band can contribute to latent charge. The latent charge can be caused by a bright star or a cosmic ray. Latent charge is a function of incident flux during a previous exposure, the time elapsed since the previous exposure and the duration of the exposure to the bright source.

To examine the latent image effect, the detector was exposed to the spectral lines of a Neon lamp in a cross-dispersed echelle spectrograph (Navarro *et al.* 2008). An echelle spectrum with the open slit is shown in the upper left image of Figure 4. The entrance slit was then closed by turning the slit mask wheel to the closed position. The mean signal of the latent images of a spectral line apparent in the subsequent 128 second dark exposures is plotted versus time in the upper curve with black diamonds in Figure 5. The first 128 second dark exposure is shown in the upper right image of Figure 4. It takes more than 10 minutes until the latent image decays. It was expected that MBE material would not exhibit any persistence, but this has not been confirmed with any of the MBE grown Hawaii-2RG arrays tested so far.

A model for image persistence was proposed by R. Smith (Smith *et al.* 2008)

which assigns this effect to charge captured by traps in the depletion region. Since infrared detectors operate in capacitive discharge mode the depletion width shrinks during the integration when photo-generated charge accumulates on the photodiode. In the upper left diagram of Figure 3 the band diagram of the pn junction is shown at the beginning of the integration at a bias voltage of -1V with electrons in red and holes in blue and the depletion region in white color. During the integration process the capacity of the diode is discharged, the depletion width shrinks and the bias voltage drops to 0 V as shown in the lower left diagram of Figure 3. In the green shaded area additional traps are exposed to mobile carriers (electrons and holes) while the integration is ongoing and some carriers may get trapped. After the depletion width is reestablished by resetting the diode, the trapped charge is slowly released in subsequent dark exposures generating a signal which is observed as latent image or persistence. The release of trapped charge is indicated in the band diagram on the right side of Figure 3.

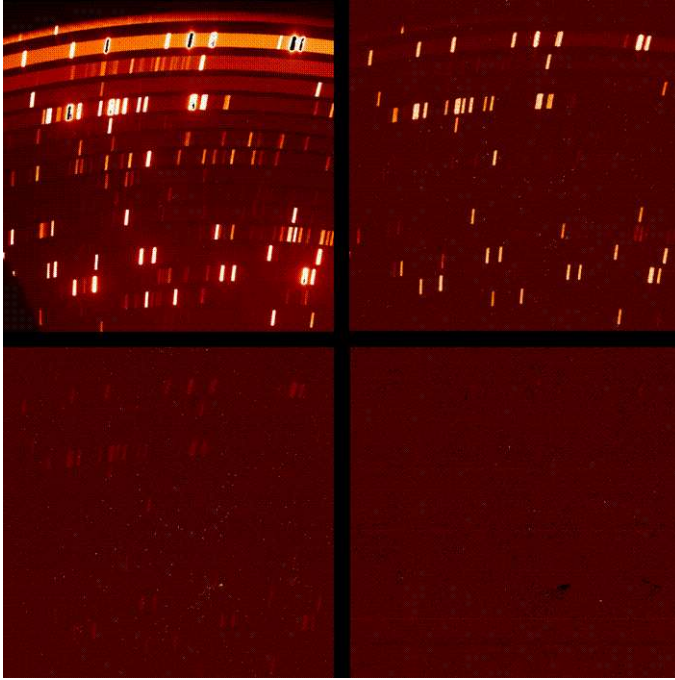


**Fig. 4.** Persistence of substrate removed MBE grown Hawaii-2RG array measured with Neon spectra in cross-dispersed echelle spectrograph. Top left: Spectrograph slit open. Top right: First 2 minute dark exposure after closure of slit with persistent images of spectral lines. Bottom left: First 2 minute dark exposure after closure of slit with two minute global reset de-trapping before closing the slit. Bottom right: First 2 minute dark exposure after closure of slit with global reset switch closed before opening slit and reset switch opened after closing slit.

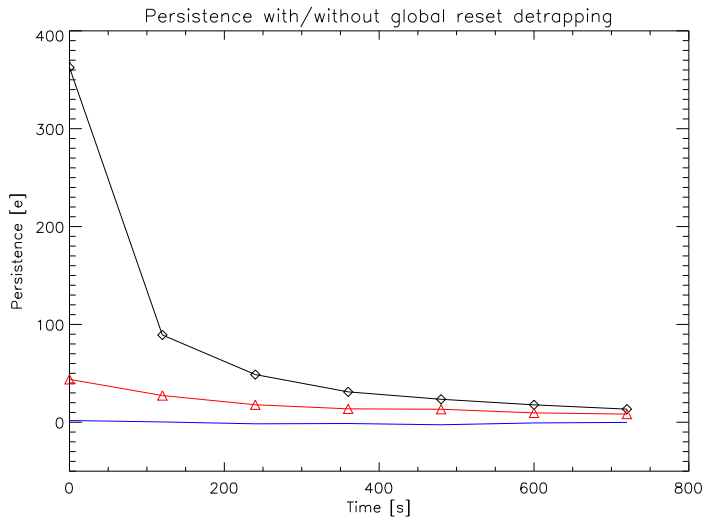


**Fig. 5.** Intensity decay of latent images in 128 s dark exposures without and with global reset de-trapping. Top curve with black diamonds: normal operation without global reset de-trapping. Middle curve with red triangles: Before closing slit global reset switch activated for 128 s to perform global reset de-trapping. Bottom blue curve: Global reset activated before opening slit and deactivated after closing slit. Integration of photons not possible with this mode.

To test the validity of the persistence model the reset switches of all pixels were closed for 128 seconds after the bright exposure was finished but before the slit was closed. The global reset feature of the Hawaii-2RG array allows to close all reset switches simultaneously. The image of the first 128 second dark exposure thus obtained is shown in the lower left image of Figure 4 and the mean signal versus time is plotted with red triangles in Figure 5. If the reset switches are closed before opening the slit and kept closed during the whole time when the slit is open, the subsequent dark exposures show no latent images as can be seen in the lower right image of Figure 4 and the blue curve at the bottom in Figure 5. Hence, closing the reset switches with the global reset may be considered as an electronic shutter protecting the detector from bright sources by preventing the depletion width to shrink. Global reset de-trapping offers a mitigation strategy for latent images with the disadvantage of additional observing overhead.

For multiplexer designs containing a capacitive transimpedance amplifier (CTIA) in the unit cell instead of a simple source follower (as implemented in the Hawaii-2RG multiplexer), the bias voltage across the detector is kept constant during the integration. Because of the fixed bias voltage the depletion width is also kept constant. Therefore, a CTIA design is expected to eliminate persistence.

#### 4 Mid infrared developments

For the mid infrared spectral region between  $\lambda = 5 \mu\text{m}$  and  $20 \mu\text{m}$  extrinsic silicon detectors are used such as Si:As, which has a cut-off wavelength of  $\lambda_c = 28 \mu\text{m}$ . In extrinsic silicon absorbed photons generate a transition from the donor level to the conduction band. To improve the quantum efficiency the Silicon has to be highly doped (D+), which generates impurity band conduction. In order to block the dark current from the D+ charge, an intrinsic blocking layer is inserted. This detector structure is called blocked impurity band (BIB) detector. For the James Webb Space Telescope JWST a 1Kx1K Si:As array called MIRI array has been developed (Love *et al.* 2004). For ground based instruments a high flux version of this detector is needed with a much larger storage capacity. This device, called the Aquarius array, is currently being developed at Raytheon. It is a 1Kx1K Si:As array which has a storage capacity of 15 million electrons, 64 parallel video output channels and can be read out at frame rates of up to 150 Hz. The unit cell design consists of a simple source follower but also offers switchable gain (storage capacities switchable between 15 million and 1 million electrons). Centered windowing is also possible. The multiplexer layout is shown in Figure 6.

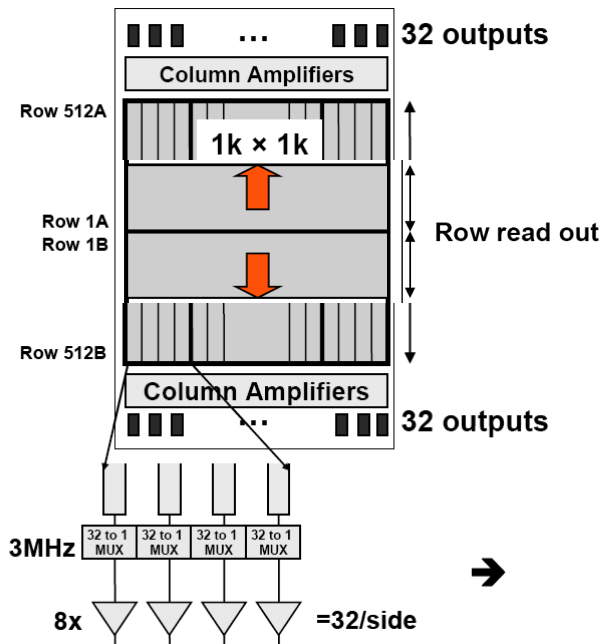


**Fig. 6.** Multiplexer layout of Aquarius 1Kx1K Si:As array with 32 channels at both top and bottom of the array. Centered window readout possible.

## 5 ASIC controller

For Hawaii-xRG arrays Teledyne has developed an ASIC controller which provides the full functionality of a conventional detector controller in a single integrated CMOS device operating at cryogenic temperatures (Loose *et al.* 2003). The ASIC is fully programmable and generates bias voltages and clocking and also digitizes the video signal of the detector on the focal plane. Hence, no cables carrying low noise analog signals have to be interfaced to the focal plane in the cryostat. The ASIC provides a choice between 36 parallel input channels each having its own preamplifier and 500 KHz 16 bit ADC or 12 channels with 10 MHz 12 bit ADCs. The power consumption is less than 150 mW for operating 32 channels at 100 KHz. The ASIC will enormously simplify the system engineering of large focal plane mosaics. The performance of the ASIC has been evaluated with a Si-PIN diode array hybridized to the Hawaii-2RG multiplexer. The noise performance achieved with the ASIC was comparable to the performance obtained with a conventional controller. For double correlated sampling the noise was 7 erms and with 30 Fowler pairs it could be reduced to 2.7 erms (Dorn *et al.* 2008). A 2x2 mosaic of  $\lambda_c=2.5 \mu\text{m}$  Hawaii-2RG arrays read out with SIDE CAR ASICs in the 32-channel mode achieved a readout noise of 12.3 erms for DCS and 4.3 erms with 16 Fowler pairs in the Four Star Instrument at the Magellan Telescope (Persson *et al.* 2008).

## 6 Fast low noise sensors

Infrared wavefront sensors for adaptive optic systems and fringe trackers for instruments used in interferometry require frame rates of up to 1 KHz. The sensors

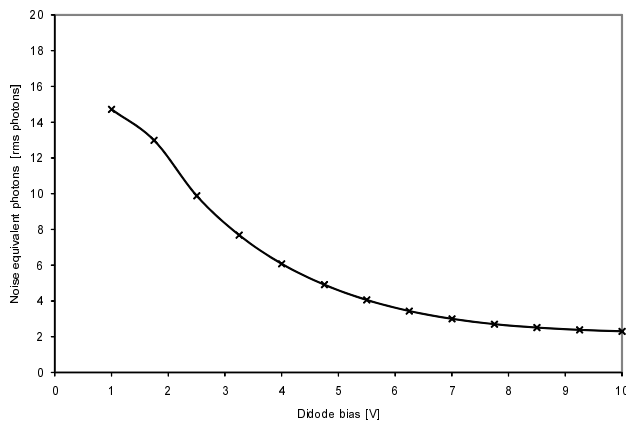


**Fig. 7.** Noise equivalent photons versus bias voltage for  $\lambda_c=2.5 \mu\text{m}$  320x256 e-APD array. Detector integration time of 1 ms. Model prediction based on measured detector parameters.

are hybrid devices with a CMOS multiplexer and  $\lambda_c=2.5 \mu\text{m}$  HgCdTe diode arrays. Due to the short integration times even bright sources generate only low signal levels, thus imposing stringent requirements on the readout noise of the sensor which has to be below a few electrons rms in order to achieve photon shot noise limited operation. For SFD (source follower per detector) unit cells the noise performance is given by the CMOS noise floor and depends on the capacitance of the integrating node, which to some extent scales with the pixel size. Current sensors employ PICNIC arrays (pixel size  $40 \mu\text{m}$ ) with a readout noise of 25 erms and Hawaii1 arrays (pixel size  $18.5 \mu\text{m}$ ) with 10 erms (Finger *et al.* 2004). To overcome the noise limitations of the CMOS SFD unit cell design two strategies have been developed.

The first strategy implies a more complex unit cell design with a capacitive transimpedance amplifier (CTIA) for each pixel, providing high gain and bandwidth. A  $128 \times 128$  pixel prototype sensor containing 7 different unit cell designs has been developed at Teledyne (Joshi *et al.* 2004). One design with a two stage CTIA called LnPix3 design which has a gain 400 corresponding to a signal of  $1.3 \text{ mV/e}$ , has been evaluated. The readout noise was between 10 and 15 erms. However, it was difficult to get uniform response and stable operation (Mehrgan *et al.* 2008). A new  $128 \times 128$  pixel detector called SPEEDSTER128 has been designed and is currently being tested at Teledyne; it has a single stage CTIA in the unit cell with a lower gain of  $0.32 \text{ mV/e}$ .

The second strategy exploits the gain provided by the electron avalanche effect of HgCdTe diodes at high reverse bias voltages. It is a well established property of HgCdTe having cut-off wavelengths between  $\lambda_c = 2$  to  $11 \mu\text{m}$  that the electron avalanche photodiode (e-APD) amplification is a deterministic, almost noiseless process (Rothman *et al.* 2007, Baker *et al.* 2004, Beck *et al.* 2006). At liquid nitrogen temperature the excess noise factor is close to unity. Since the impact ionization coefficient for the electrons is much larger than for holes, the avalanche gain is a pure electron process. The APD gain is an exponential function of bias voltage. For  $\lambda_c = 5 \mu\text{m}$  material gains of  $>1000$  have been measured at a moderate bias voltage of 11 V without onset of avalanche breakdown and excellent gain uniformity (Rothman *et al.* 2007). SELEX has already developed a  $320 \times 256$  element eAPD array with a  $24 \mu\text{m}$  pixel pitch and a cut-off wavelength of  $\lambda_c=4.5 \mu\text{m}$ . The array is integrated in a laser gated imaging system with a Nd YAG laser producing 20 ns pulses. The array achieves sensitivities as low as 10 photons rms. Since a wavefront sensor operates with much longer integration times of about 1 ms, the performance of  $\lambda_c=4.5 \mu\text{m}$  HgCdTe material is limited by the shot noise of the detector dark current. For this reason a pre-development study was carried out at SELEX to explore the reduction of dark current for HgCdTe eAPD arrays having the cut-off wavelength changed from  $\lambda_c=4.5 \mu\text{m}$  to  $\lambda_c=2.5 \mu\text{m}$  and investigate their potential for infrared wavefront sensing. First arrays have been produced and will be evaluated. A model using measured detector parameters such as dark current and CMOS source follower noise has been used to predict the noise performance for detector integration times of 1 ms. The noise performance as a function of bias voltage is shown in Figure 7. At high bias voltages the e-APD

gain reduces the noise expressed in noise equivalent photons to values as low as 2.3 noise equivalent photons.

Detector architectures have been proposed to operate the e-APD arrays in Geiger mode and build a noiseless high quantum efficiency photon counting infrared array. Each pixel has a counter in its unit cell and at the end of the exposure only the digital numbers stored in the registers of the pixel counters are read out. In this way the readout noise is completely eliminated. If the region where photons are absorbed and charge is generated and the gain region with the Geiger APD can be well separated to keep the dark current low this readout scheme may also be applied to low flux applications. It would provide sensitivities which are only limited by the Poisson statistics of the observed target.

## 7 Conclusions

In the near infrared large format HgCdTe arrays have evolved with formats up to 4Kx4K pixels. The format of the arrays is limited by the detector substrate and larger formats are implemented as mosaics. The pixel performance approaches theoretical limits. An unsolved problem is the detector persistence for detectors having a multiplexer with an SFD unit cell operating in capacitive discharge mode. The persistence is attributed to traps in the depletion region of the diode junction. Detectors having a CTIA in the unit cell should not suffer from persistence since the depletion width of the diode junction is kept constant. Global reset de-trapping is a mitigation strategy for SFD arrays. A new Si:As BIB array is developed for ground based MID infrared applications. Fast low noise sensors are being developed using CMOS multiplexers with CTIA designs. An alternative approach is the development of e-APD arrays. HgCdTe e-APD's offer noiseless gain to overcome the noise limitations imposed by CMOS multiplexers.

## References

- Finger G. *et al.* 2008, Proc. SPIE 7021, to be published.  
Smith R. M. *et al.* 2008, Proc. SPIE 7021, to be published.  
Love, P. *et al.* 2004, Proc. SPIE, Vol. 5499, 86.  
Garnett, J. *et al.* 2004, Scientific Detectors for Astronomy 2002, edited by Amico P. and Beletic J. , 59.  
Love, P., Hoffman, A. *et al.* 2006, Scientific Detectors for Astronomy 2005, edited by Beletic J. , 411.  
Navarro R. *et al.* 2008, Proc. SPIE 7014, to be published.  
Loose M. *et al.* 2003, Proc. SPIE 4841, 782.  
Dorn R. *et al.* 2008, Proc. SPIE 7021, to be published.  
Persson S. E. *et al.* 2008, Proc. SPIE 7014, 95.  
Finger G. *et al.* 2004, Proc. SPIE 5499, 97.  
Joshi A. *et al.* 2004, Proc. SPIE 5499, 228.  
Mehrgan L. *et al.* 2008, Proc. SPIE 7021, to be published.

Rothman J. *et al.* 2007, Proc. SPIE 6542, 654219.

Baker I. *et al.* 2004, Proc. SPIE, Vol. 5406, 133.

Beck J. I. *et al.* 2006, J. Electron. Materials, 35, 1166.